ADVANCED ENERGY MATERIALS

Supporting Information

for *Adv. Energy Mater.,* DOI: 10.1002/aenm.202201939

Oxide-Based Solid-State Batteries: A Perspective on Composite Cathode Architecture

Yaoyu Ren, Timo Danner, Alexandra Moy, Martin Finsterbusch, Tanner Hamann, Jan Dippell, Till Fuchs, Marius Müller, Ricky Hoft, André Weber, Larry A. Curtiss, Peter Zapol, Matthew Klenk, Anh T. Ngo, Pallab Barai, Brandon C. Wood, Rongpei Shi, Liwen F. Wan, Tae Wook Heo, Martin Engels, Jagjit Nanda, Felix H. Richter, Arnulf Latz, Venkat Srinivasan, Jürgen Janek,* Jeff Sakamoto,* Eric D. Wachsman,* and Dina Fattakhova-Rohlfing**

Supplementary information

Oxide-Based Solid-State Batteries: A Perspective on Composite Cathode Architecture

Yaoyu Ren, Timo Danner, Alexandra Moy, Martin Finsterbusch, Tanner Hamann, Jan Dippell, Till Fuchs, Marius Müller, Ricky Hoft, André Weber, Larry A. Curtiss, Peter Zapol, Matthew Klenk, Anh T. Ngo, Pallab Barai, Brandon Wood, Rongpei Shi, Liwen F. Wan, Tae Wook, Martin Engels, Jagjit Nanda, Felix H. Richter, Arnulf Latz, Venkat Srinivasan, Jürgen Janek, Jeff Sakamoto, Eric Wachsman, Dina Fattakhova-Rohlfing

1 Thermodynamic calculations of the energy density of LLZO based cells

1.1 Description of cell design

Thermodynamic energy densities were calculated for the following battery design:

1. Electrolyte = LLZO bilayer
    a. LLZO dense layer = 0 % porosity, 10 µm thick
    b. LLZO porous layer = 75 % porosity, variable thickness (1-100 µm thick)
2. Anode = Li-metal
    a. Attached directly to LLZO dense layer
3. Cathode active material = LCO, NMC622, NMC811, Sulfur, FeF_3, Li-air
    a. Fills pore volume within LLZO porous layer
    b. Electronic additive (if applicable) = Graphite, variable amount
    c. Remaining empty pore = variable amount

1.2 Calculation procedure

Thermodynamic energy densities were calculated using the following approach:

1. Select total cathode layer thickness “L”
2. Based on porosity “P” of LLZO porous layer, calculate available pore volume “L*P” (assuming a battery area of 1 cm^2)
3. Fill pore volume with cathode active material and Electronic additive (if applicable):

a. Cathode active material only
    i. LCO, NMC622, NMC811 = 100 % pore filling
    ii. Sulfur = 55.96 % pore filling
    iii. FeF_3 = 87.66 % pore filling
    iv. Li-air = 100 % pore filling (as Li_2O_2)
b. Cathode active material and Electronic additive
    i. LCO = 90.78 % pore filling, Electronic additive = 9.22 % pore filling
    ii. NMC622 = 91.26 % pore filling, Electronic additive = 8.74 % pore filling
    iii. NMC811 = 91.07 % pore filling, Electronic additive = 8.93 % pore filling
    iv. Sulfur = 49.34 % pore filling, Electronic additive = 11.82 % pore filling
    v. FeF_3 = 60.41 % pore filling, Electronic additive = 31.09 % pore filling
    vi. Li-air = 88.89 % pore filling (as Li_2O_2), Electronic additive = 11.11 % pore filling

4. Capacity match Li-metal anode to total capacity of cathode active material in LLZO porous layer
5. Calculate total battery mass
    a. Cathode active material mass
        i. LCO, NMC622, NMC811, Sulfur, FeF_3 = keep mass of cathode active material in total battery mass
        ii. Li-air = remove mass of cathode active material (Li_2O_2) from total battery mass
            1. Total battery mass is calculated when all Li is contained in Li-metal anode and no Li_2O_2 is present
    b. Electronic additive mass (if applicable)
    c. LLZO porous layer mass
    d. LLZO dense layer mass
    e. Li-metal anode mass
        i. LCO, NMC622, NMC811 = remove mass of Li-metal anode from total battery mass
        1. Cathode active material contains all Li used during cycling
        ii. Sulfur, FeF_3 = keep mass of Li-metal anode in total battery mass

1. Cathode active material contains no Li

iii. Li-air = keep mass of Li-metal anode in total battery mass

1. Total battery mass is calculated when all Li is contained in Li-metal anode and no Li_2O_2 is present

6. Calculate total battery volume
    a. LLZO porous layer volume = "L" (assuming a battery area of 1 cm^2)
        i. Cathode active material and Electronic additive are completely contained inside the pores of the LLZO porous layer
        ii. Therefore, use the outer boundary of the LLZO porous layer and calculate the volume of this entire region
    b. LLZO dense layer volume
    c. Li-metal anode volume
        i. LCO, NMC622, NMC811 = remove volume of Li-metal anode from total battery volume

1. Cathode active material contains all Li used during cycling

ii. Sulfur, FeF_3 = keep volume of Li-metal anode in total battery volume

1. Cathode active material contains no Li

iii. Li-air = keep volume of Li-metal anode in total battery volume

1. Total battery volume is calculated when all Li is contained in Li-metal anode and no Li_2O_2 is present

1.3 Material parameters

Thermodynamic energy densities were calculated using the following material properties:

Electrolyte

- LLZO = $Li_7La_3Zr_2O_{12}$
    - Mass density = 5.077 g/cm^3
        - Calculated for cubic lattice with 13.00 Å lattice parameter, 8 formula units per unit cell

Anode

- Li-metal

- Mass density = 0.534 g/cm^3
- Molecular weight = 6.941 g/mol
- Specific capacity = 3861.3 mAh/g

Cathode active material

- **LCO = $LiCoO_2$**
  - Material change = $LiCoO_2 \leftrightarrow Li_{0.5}CoO_2$
  - Mass density = 5.046 g/cm^3
    - Calculated from molar density of 51555 mol/m^3 (Ramadass et al., Development of First Principles Capacity Fade Model for Li-Ion Cells, J. Electrochem. Soc., 151 (2) A196-A203 (2004). 10.1149/1.1634273)
  - Molecular weight = 97.87 g/mol
  - Specific capacity = 142.1 mAh/g (between 4.3 and 3 V)
    - Ramadass et al., Development of First Principles Capacity Fade Model for Li-Ion Cells, J. Electrochem. Soc., 151 (2) A196-A203 (2004). 10.1149/1.1634273
    - 0.519 mol Li per mol LCO
  - Average discharge voltage = 3.96 V (vs. Li/Li+) (between 4.3 and 3 V)
    - Ramadass et al., Development of First Principles Capacity Fade Model for Li-Ion Cells, J. Electrochem. Soc., 151 (2) A196-A203 (2004). 10.1149/1.1634273
  - Conductive additive = graphite
    - 4.17 wt% graphite, 95.83 wt% LCO
    - Based on 92/4/4 wt% for LCO/Electronic additive/PVDF, but with PVDF component removed

- **NMC622 = $LiNi_{0.6}Mn_{0.2}Co_{0.2}O_2$**
  - Material change = $LiNi_{0.6}Mn_{0.2}Co_{0.2}O_2 \leftrightarrow Li_{1-x}Ni_{0.6}Mn_{0.2}Co_{0.2}O_2$
  - Average mass density = 4.76 g/cm^3

        - 4.74 g/cm^3= Schreiner, D., Klinger, A. & Reinhart, G. Modeling of the calendering process for lithium-ion batteries with DEM simulation. Procedia CIRP 93, 149–155 (2020).
        - 4.78 g/cm^3= Zheng, L., Hatchard, T. D. & Obrovac, M. N. A high-quality mechanofusion coating for enhancing lithium-ion battery cathode material performance. MRS Commun. 9, 245–250 (2019).
    - Molecular weight = 96.93 g/mol
    - Specific capacity = 184.1 mAh/g (between 4.3 and 3 V)
        - Ahmed, S. et al. Cost of automotive lithium-ion batteries operating at high upper cutoff voltages. J. Power Sources 403, 56–65 (2018).
        - 0.666 mol Li per mol NMC622
    - Average discharge voltage = 3.82 V (vs. Li/Li+) (between 4.3 and 3 V)
        - Ahmed, S. et al. Cost of automotive lithium-ion batteries operating at high upper cutoff voltages. J. Power Sources 403, 56–65 (2018).
    - Conductive additive = graphite
        - 4.17 wt% graphite, 95.83 wt% NMC622
        - Based on 92/4/4 wt% for NMC622/Electronic additive/PVDF, but with PVDF component removed

- **NMC811 = $LiNi_{0.8}Mn_{0.1}Co_{0.1}O_2$**
    - Material change = $LiNi_{0.8}Mn_{0.1}Co_{0.1}O_2 \leftrightarrow Li_{1-x}Ni_{0.8}Mn_{0.1}Co_{0.1}O_2$
    - Average mass density = 4.87 g/cm^3
        - Sturm, J. et al. Modeling and simulation of inhomogeneities in a 18650 nickel-rich, silicon-graphite lithium-ion cell during fast charging. J. Power Sources 412, 204–223 (2019).
    - Molecular weight = 97.28 g/mol
    - Specific capacity = 218.7 mAh/g (between 4.3 and 3 V)
        - Sturm, J. et al. Modeling and simulation of inhomogeneities in a 18650 nickel-rich, silicon-graphite lithium-ion cell during fast charging. J. Power Sources 412, 204–223 (2019).
        - 0.794 mol Li per mol NMC811

- Average discharge voltage = 3.86 V (vs. Li/Li+) (between 4.3 and 3 V)
    - Sturm, J. et al. Modeling and simulation of inhomogeneities in a 18650 nickel-rich, silicon-graphite lithium-ion cell during fast charging. J. Power Sources 412, 204–223 (2019).
- Conductive additive = graphite
    - 4.17 wt% graphite, 95.83 wt% NMC811
    - Based on 92/4/4 wt% for NMC811/Electronic additive/PVDF, but with PVDF component removed

- **Sulfur**
    - Material change = S ←→ Li_2S
    - Mass density (Sulfur)= 2.07 g/cm^3
    - Molecular weight (Sulfur) = 32.065 g/mol
    - Mass density (Li_2S) = 1.66 g/cm3
    - Molecular weight (Li_2S) = 45.95 g/cm^3
    - S to Li_2S volume expansion = 78.70%
    - Specific capacity (vs Sulfur mass only) = 1671.7 mAh/g
        - 2 mol Li per mol Li_2S
    - Average discharge voltage = 2.2 V (vs. Li/Li+)
        - Fang, R. et al. More Reliable Lithium-Sulfur Batteries: Status, Solutions and Prospects. Adv. Mater. 29, 1606823 (2017).
    - Conductive additive = graphite
        - 20 wt% graphite, 80 wt% Sulfur
            - Chung, S.-H., Chang, C.-H. & Manthiram, A. Progress on the Critical Parameters for Lithium-Sulfur Batteries to be Practically Viable. Adv. Funct. Mater. 28, 1801188 (2018).

- **FeF_3**
    - Material change = FeF_3 ←→ Fe + 3LiF
    - Mass density (FeF_3) = 3.52 g/cm^3

        - Wang, L. et al. Li-free Cathode Materials for High Energy Density Lithium Batteries. Joule 3, 2086–2102 (2019).
    - Molecular weight (FeF_3) = 112.84 g/mol
    - Mass density (Fe + 3LiF) = 3.6551 g/cm^3
    - Molecular weight (Fe + 3LiF) = 133.66 g/mol
    - FeF_3 to (Fe + 3LiF) volume expansion = 14.07%
    - Specific capacity (vs. FeF_3 mass only) = 712.6 mAh/g
        - 3 mol Li per mol (Fe + 3LiF)
    - Average discharge voltage = 2.74 V (vs. Li/Li+)
        - Wang, L. et al. Li-free Cathode Materials for High Energy Density Lithium Batteries. Joule 3, 2086–2102 (2019).
    - Conductive additive = graphite
        - 24 wt% graphite, 76 wt% FeF_3
            - Wu, F. et al. 3D Honeycomb Architecture Enables a High-Rate and Long-Life Iron (III) Fluoride–Lithium Battery. Adv. Mater. 31, 1–9 (2019).
            - Only kept carbon that was initially ball milled with FeF_3
            - Did not keep additional carbon used to make cathode slurry

- **Li-air**
    - Material change = empty ←→ Li_2O_2
    - Mass density (Li_2O_2) = 2.31 g/cm^3
    - Molecular weight (Li_2O_2) = 45.881 g/mol
    - Specific capacity = 1168.3 mAh/g
        - 2 mol Li per mol Li_2O_2
    - Average discharge voltage = 2.96 V (vs. Li/Li+)
        - Chase, M. W. Jr. NIST-JANAF THERMOCHEMICAL TABLES, Fourth Edition, Monograph 9 (Part I and Part II). in Journal of Physical and Chemical Reference Data Monographs or Supplements 1510 (1998).
    - Conductive additive = graphite

        - 10.46 wt% graphite, 89.54 wt% Li_2O_2
            - Zhu, X., Zhao, T., Tan, P., Wei, Z. & Wu, M. A high-performance solid-state lithium-oxygen battery with a ceramic-Electronic nanostructured electrode. Nano Energy 26, 565–576 (2016).
            - Based on carbon catalyst (10,000 mAhr/g specific capacity)

Electronic additive

- Graphite
    - Mass density = 2.16 g/cm^3

2 Dynamic assessment of LLZO based cells

Specific energy calculations are based on simulations with a pseudo-2D model [14] following the formulation presented in [3] for state-of-the-art LIBs with liquid electrolyte. The model was adopted for a better representation of the processes in LLZO based cells. Constitutive equations are summarized in Table 1. The main assumptions and features will be briefly described in the following paragraph.

2.1 Model description

Following the ASSB cell design suggested for the calculation of specific energies in the previous paragraph the simulation domain consists of a composite cathode made of cathode active material (CAM) and LLZO solid electrolyte, a dense solid electrolyte pellet, and a lithium metal anode. In the cathode the CAM and LLZO form a percolating network for electron (Eq. (1)) and ion (Eq. (2)) transport allowing full utilization of the active material. The thickness of the composite electrode is set to 50 and 100 µm and the CAM content is fixed to 75 vol-%.

Table 1 - Model equations of pseudo-2D model adopted for the simulation of LLZO based cells

	CAM	LLZO	Li
Charge Balance	$ai_{se} = \frac{\partial}{\partial x}\left(\kappa_{eff}\frac{\partial}{\partial x}\Phi_s\right)$ (1)	$-ai_{se} = \frac{\partial}{\partial x}\left(\sigma_{Li,eff}\frac{\partial}{\partial x}\Phi_e\right)$ (2)	-
Mass Balance	$\frac{\partial c_s}{\partial t} + \frac{1}{r^2}\frac{\partial}{\partial r}\left(r^2\left(-D_{Li}^{CAM}\frac{\partial c_s}{\partial r}\right)\right) = 0$ (3)	-	-
Interface condition	$i_{se} = 2 \cdot i_{00}^{CAM} \cdot \sqrt{c_{So}} \cdot sinh\left(\frac{F}{2RT}\eta\right)$ (4) $\eta = \Phi_S - \Phi_E - U_0^{CAM}(c_S) - i_{se} \cdot R_{SP}$ (5)		
Interface condition		$i_{Li} = 2 \cdot i_{00}^{Li} \cdot sinh\left(\frac{F}{2RT}(\Phi_{Li} - \Phi_E)\right)$ (6)	

In the cathode the CAM and LLZO form a percolating network for electron (Eq. (1)) and ion (Eq. (2)) transport allowing full utilization of the active material. We assume a completely dense

composite after sintering without any porosity. Moreover, the electrodes do not contain additional conductive additives. Therefore, the effective electronic conductivity of the composite electrode is given by

$$\kappa_{eff} = \varepsilon_{CAM}^{\beta_s} \kappa_{CAM}(c_s), \tag{7}$$

where κ_{CAM} is calculated as the integral average of the concentration dependent conductivity $\kappa_{CAM}^0(c_s)$ over the radius of representative CAM particles. The Bruggeman coefficient $\beta_s$representing the tortuosity of the CAM phase with volume fraction ε_{CAM} is in all scenarios set to a constant value of 2.3 [10]. In our simulations we assume that LLZO is a single-ion conductor. Therefore, the ionic current in the solid electrolyte is given by $j_{Li}^{LLZO} = -\sigma_{Li,eff} \frac{\partial}{\partial x} \Phi_e$and the flux of lithium ions follows as N_{Li}^{LLZO}/F. The effective ionic conductivity of the composite electrode is calculated according to

$$\sigma_{Li,eff} = \varepsilon_{LLZO}^{\beta_e} \sigma_{LLZO}^0 \,. \tag{8}$$

The exponent $\beta_e = \beta_{GB} + \beta_{tort}$. includes the reduction of the bulk conductivity σ_{LLZO}^0 due to the tortuosity of transport pathways β_{tort} in the LLZO phase with volume fraction ε_{LLZO} as well as contributions of secondary phases and grain boundaries β_{GB}.

The charge transfer reaction at the surface of CAM particles is described by Eq. (4) and (5) which also provides the flux of lithium used as boundary condition in Eq. (3). The exchange current density factor i_{00}^{CAM} is calculated from the area specific resistance ($R_{CT,CAM}$) assuming linearized kinetics at low overpotentials according to

$$i_{00}^{CAM} = \frac{1}{\mathrm{R_{CT,CAM}}} \frac{RT}{F} \frac{1}{c_{max}^{CAM\,0.5}} \tag{9}$$

c_{max}^{CAM} is the maximum lithium concentration given by the molecular weight and density of the CAM. R, F, and T are the ideal gas constant, Faraday constant and cell temperature, respectively. All predictions are done for room temperature operation. Note, that we use in our simulations a Butler-Volmer type kinetic expression for the Faradaic processes at the interface with a non-linear relationship between current and overpotential. The linearization step is only done for the parametrization of i_{00}^{CAM} by impedance data. If passivating layers of degradation products limit the ion transport towards the interface the resistance determined by R_{SP} (Eq. (5)) governs the interface kinetics at high currents.

Neglecting resistive interphases, the exchange current density of the lithium plating and stripping reaction at the anode is calculated according to

$$i_{00}^{Li} = \frac{1}{R_{CT,Li}} \frac{RT}{F}. \quad (10)$$

Electrochemical and mechanical degradation processes are also neglected in the simulations.

2.2 Model parametrization

Material parameters are compiled from various sources in the literature. Table 3 in the main manuscript provides an overview of the parameters in the different scenarios presented in this work including the corresponding literature. Material parameters of CAMs are given as function of lithium concentration. Correlations were adjusted to data published in the literature. Material parameters as function of specific capacity are presented in Figure SI-1.

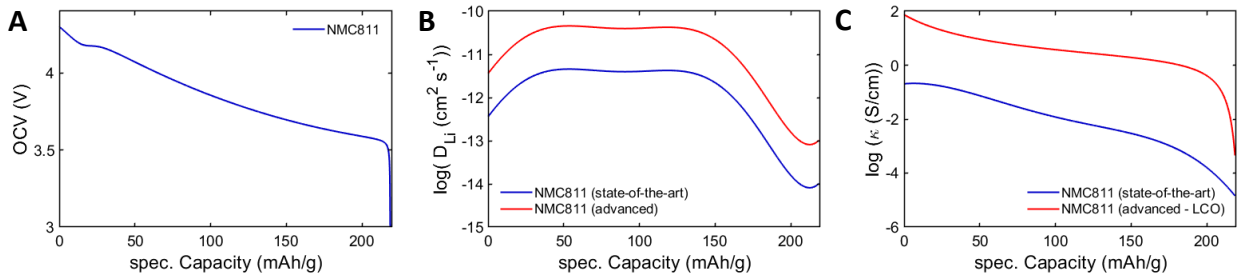

Figure SI-1 – Correlations of material properties as function of lithium content. a) Open circuit voltage of NMC811 [2] b) Chemical diffusion coefficient of Li in NMC811 [5]. Parameters of the optimized NMC811 adjusted based on [5,13]. c) Electronic conductivity of NMC811 [8,9]. Conductivity of the advanced case corresponds to the conductivity of LCO [7].

2.3 Additional simulation results

Figure SI-2 presents an overview of the simulated 'State-of-the-art' scenario presented in Figure 7.3d in the main manuscript. Note, that the configuration presented in the main manuscript has a CAM content of 75 vol-% and an electrode thickness of 50 and 100 µm, respectively. Generally, CAM contents larger than 65 vol-% are required for theoretical specific energies larger than 500 Wh/kg. However, limitations due to Li transport in LLZO favor lower CAM contents when using state-of-the-art materials. For a lithiation current of 1 mA/cm^2 an optimum was found at around 65 vol-% reaching up to 2 times the specific

energy of the configuration presented in the main manuscript. This result highlights the potential of electrode engineering. If transport in the SE is improved (case ‘Improved materials’) the optimal design follows the trend in the thermodynamic calculations with optimal specific energy at high CAM loadings.

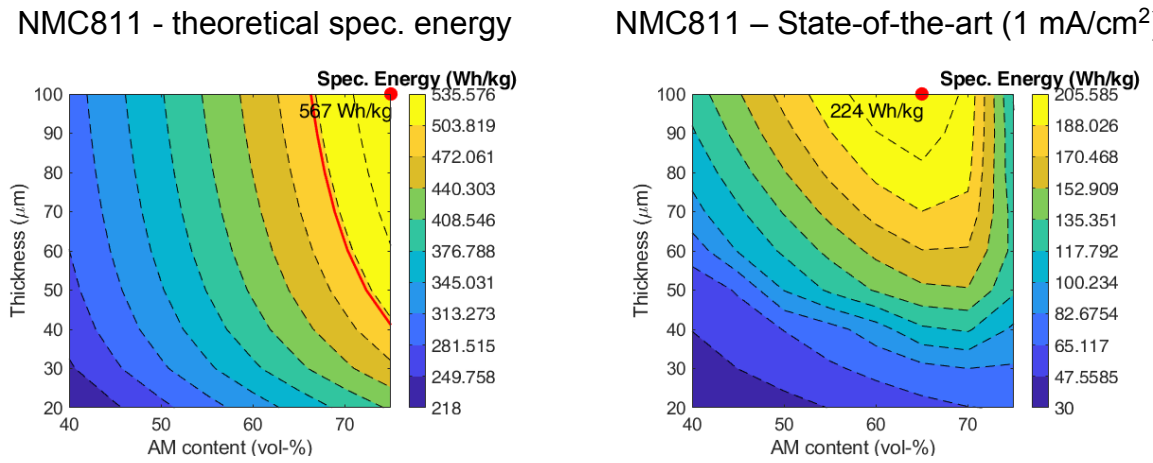

Figure SI-2: Overview of the theoretical and simulated specific energies for different composite electrode designs using the state-of-the-art scenario.

3 References

[1] Akimoto, J., Gotoh, Y. & Oosawa, Y. Synthesis and Structure Refinement of LiCoO2 Single Crystals. J. Solid State Chem. 141, 298–302 (1998). https://doi.org/10.1006/jssc.1998.7966

[2] Sturm, J. et al. Modeling and simulation of inhomogeneities in a 18650 nickel-rich, silicon-graphite lithium-ion cell during fast charging. J. Power Sources 412, 204–223 (2019). https://doi.org/10.1016/j.jpowsour.2018.11.043

[3] Ramadass et al., Development of First Principles Capacity Fade Model for Li-Ion Cells, J. Electrochem. Soc., 151 (2) A196-A203 (2004). 10.1149/1.1634273

[4] R. Mücke et al., Modelling electro-chemical induced stresses in all-solid-state batteries: Anisotropy effects in cathodes and cell design optimization, https://doi.org/10.1016/j.jpowsour.2020.229430

[5] R. Ruess et al., Influence of NCM Particle Cracking on Kinetics of Lithium-Ion Batteries with Liquid or Solid Electrolyte, *J. Electrochem. Soc.* **167** 100532 (2020). https://doi.org/10.1149/1945-7111/ab9a2c

[6] Kato et al., In-situ Li7La3Zr2O12/LiCoO2 interface modification for advanced all-solid-state battery, J. Power Sources 260 (2014) 292-298, http://dx.doi.org/10.1016/j.jpowsour.2014.02.102

[7] Molenda et al., Modification in the electronic structure of cobalt bronze Li_xCoO_2 and the resulting electrochemical properties, https://doi.org/10.1016/0167-2738(89)90058-1

[8] Amin et al., Characterization of Electronic and Ionic Transport in Li1-xNi0.33Mn0.33Co0.33O2 (NMC333) and Li1-xNi0.50Mn0.20Co0.30O2 (NMC523) as a Function of Li Content, J. *Electrochem. Soc*, **163** (8) A1512-A1517 (2016), 10.1149/2.0131608jes

[9] Noh, H. J., Youn, S., Yoon, C. S., & Sun, Y. K. (2013). Comparison of the structural and electrochemical properties of layered $Li[Ni_xCo_yMn_z]O_2$ (x = 1/3, 0.5, 0.6, 0.7, 0.8 and 0.85) cathode material for lithium-ion batteries. *Journal of Power Sources*, *233*, 121-130. https://doi.org/10.1016/j.jpowsour.2013.01.063

[10] Neumann et al., Effect of the 3D Structure and Grain Boundaries on Lithium Transport in Garnet Solid Electrolytes, ACS Appl. Energy Mater. 2021, 4, 4786−4804, https://doi.org/10.1021/acsaem.1c00362

[11] Qin et al. Growth of self-textured Ga31-substituted Li7La3Zr2O12 ceramics by solid state reaction and their significant enhancement in ionic conductivity, APPLIED PHYSICS LETTERS 112, 113901 (2018), https://doi.org/10.1063/1.5019179.
[12] M. Finsterbusch et al., High Capacity Garnet-Based All-Solid-State Lithium Batteries: Fabrication and 3D-Microstructure Resolved Modeling, ACS Appl. Mater. Interfaces 2018, 10, 26, 22329–22339. https://doi.org/10.1021/acsami.8b06705
[13] Wang et al., Single crystal cathodes enabling high-performance all-solid-state lithium-ion batteries, Energy Storage Materials 30 (2020) 98–103, https://doi.org/10.1016/j.ensm.2020.05.007
[14] M. Doyle et al., Modeling of Galvanostatic Charge and Discharge of the Lithium/Polymer/Insertion Cell, J. Electrochem. Soc. (1993) 140 1526. https://doi.org/10.1149/1.2221597